Received: 24 February 2023 | Accepted: 14 February 2024

DOI: 10.1002/vzj2.20321

Vadose Zone Journal

ORIGINAL ARTICLE

Elucidating the role of water films on solute diffusion in unsaturated porous media by improved pore-scale modeling

Yuankai Yang[1] | **Ravi A. Patel**[2] | **Nikolaos I. Prasianakis**[3] | **Sergey V. Churakov**[3,4] | **Guido Deissmann**[1] | **Dirk Bosbach**[1]

[1]Institute of Energy and Climate Research (IEK-6): Nuclear Waste Management, and JARA-CSD, Forschungszentrum Jülich GmbH, Jülich, Germany

[2]Institute of Building Materials and Concrete Structures (IMB), Karlsruhe Institute of Technology (KIT), Karlsruhe, Germany

[3]Laboratory for Waste Management, Paul Scherrer Institut, Villigen, Switzerland

[4]Institute of Geological Sciences, University of Bern, Bern, Switzerland

Correspondence
Yuankai Yang, Institute of Energy and Climate Research (IEK-6): Nuclear Waste Management, and JARA-CSD, Forschungszentrum Jülich GmbH, 52425, Jülich, Germany.
Email: y.yang@fz-juelich.de

Assigned to Associate Editor Ute Wollschläger.

Funding information
Innovation and Networking Fund of the Helmholtz Association, Grant/Award Number: SO-093-iCross; Horizon 2020 Framework Programme, Grant/Award Number: 847593; Bundesministerium für Bildung und Forschung, Grant/Award Number: 02NUK053A

Abstract

Solute diffusion in partially saturated porous media is an important fundamental process in many natural and environmental systems. At low water saturation, the solute transport is governed by the diffusion in thin water films on the surfaces of solids. In this study, we established an improved pore-scale simulation framework successfully describing the solute diffusion in variably saturated porous media (e.g., soils), which considers the contribution of the diffusion within the thin water film on the surface of the solid matrix. The model takes into account the liquid–gas distribution in the underlying porous media by the Shan-Chen lattice Boltzmann Method (LBM) and simulates the solute diffusion in the bulk liquid phase and the water film. Based on the numerical results, an easy-to-use theoretical formula was also developed to predict the effective diffusivity in microporous materials at low saturation levels. The average relative error of its prediction with respect to the experimental data from the literature is about 30%, while that of the classical power law exceeds 70%. A simple phase diagram was defined, which allows us to identify the situations under which it is necessary to take the influence of surface water films on the effective diffusivity in unsaturated microporous media into account. The present study improves the pore-scale model to address solute diffusion in the water films at low water saturation and elucidates the contribution of thin water films on solute transport.

1 | INTRODUCTION

The transport of solutes in variably saturated porous media is a fundamental process relevant to various technical and natural systems. Critical examples include contaminant transport in

Abbreviations: D3Q19, three-dimensional nineteenth speed; D3Q7, three-dimensional seventh speed; LBM, lattice Boltzmann method; QSGS, quartet structure generation set.

soils and the vadose zone (Hu et al., 2004; Mehta et al., 1995; Olesen et al., 1999) and radionuclide migration in the context of nuclear waste disposal (Savoye et al., 2010, 2012). In the past decades, an extensive number of experiments (Badv & Faridfard, 2005; Hamamoto et al., 2009; Savoye et al., 2012; So & Nye, 1989; Tokunaga et al., 2017) and modeling studies (Genty & Pot, 2014; Gimmi & Churakov, 2019; Hunt et al., 2014; Yoon et al., 2015) have provided enhanced understanding and predictions of the solute transport in partially saturated complex porous media such as soils, clay rocks, and crystalline rocks.

The diffusive flux J of a dissolved solute in the aqueous solutions filling porous materials can be described with Fick's law, which shows a linear relationship to the concentration gradient ∇C as $J = D_e \nabla C$, with D_e being the effective diffusion coefficient (Hornung, 1997). Therefore, the effective diffusion coefficient D_e is a critical parameter controlling the Fickian diffusion of solutes through porous media. The value of D_e in partially saturated porous media depends on different factors such as porosity θ, degree of saturation S_w, aqueous molecular-diffusion coefficient D_0, as well as the connectivity of the water phase in the porous material. Previous studies (Hu & Wang, 2003; Millington & Quirk, 1961; Revil & Jougnot, 2008) commonly predict the values of normalized effective diffusivities D_e^* from an extension of Archie's law given as: $D_e^* = D_e/D_0 = \theta^n S_w^m$, where the two empirical parameters n and m are determined by fitting to experimental data. Furthermore, by assuming $n = m$, the above equation can be simplified to a power-law form as (Chou et al., 2012):

$$D_e^* = D_e/D_0 = \left(S_w\theta\right)^{\mathrm{n}} = \varphi^{\mathrm{n}}, \tag{1}$$

where $\varphi = S_w\theta$ denotes the volumetric water content. Further, a modified version of this power law was proposed with an additional constant k (Brooks & Corey, 1966; Mehta et al., 1995),

$$D_e^* = k\varphi^{\mathrm{n}}. \tag{2}$$

In this concept, considering a nonvolatile solute, the gas and solid phases are inaccessible, and the solute is only present in the liquid phase. Hence, φ can be treated as the accessible volumetric fraction of water or nonvolatile solutes in unsaturated porous media. Figure 1 summarizes previously measured effective diffusivities in soils as a function of water contents (Barraclough & Tinker, 1981; Conca & Wright, 1992; Klute & Letey, 1958; Romkens & Bruce, 1964; Rowell et al., 1967; So & Nye, 1989; Tokunaga et al., 2017). By fitting Equation (2) with these experimental data, the parameters of Equation (2) were determined and the corresponding best-fitting curve $D_e^* = 1.51\varphi^{2.03}$ is also plotted (cf. red line in Figure 1). It indicates that D_e^* derived from experiments decreases almost linearly with the reduction of φ at higher water saturation levels (e.g., $\varphi > 0.3$). However, the best-fitting curve overestimates D_e^* in comparison with experimental data at $\varphi > 0.4$. When the water content is below 0.3 ($\varphi \leq 0.3$), the experimental points show more significant divergence. If the water content drops below 0.2 ($\varphi < 0.2$), the measured D_e^* shows a strongly nonlinear and rapid decrease. The accuracy of the fitting power-law equation (cf. red line in Figure 1) is questionable. Specifically, the fitting equation significantly underestimates the experimental data from Tokunaga et al. (2017) (cf. black squares in Figure 1). Even at a very low water content, D_e^* is still nonzero since the hydrophilic mineral surfaces are still wetted by a thin water film providing a connected transport pathway for solutes. To capture such a complex behavior, several groups (Fityus et al., 1999; Mehta et al., 1995; Olesen et al., 1999) have proposed a two-component model including transport in saturated and partially saturated pores.

Thanks to the recent developments in advanced microscopic observation techniques and high-performance computing, pore-scale studies can be used nowadays to reconstruct the microscopic distribution of liquid and gas phases in real three-dimensional (3D) pore geometries (Pot et al., 2015), and further investigate the spatiotemporal behavior of solute transport in such unsaturated media (Genty & Pot, 2014; Hasan et al., 2020; He et al., 2017; Qiu et al., 2012; Raoof et al., 2010). In contrast to empirical models, 3D pore-scale simulations can provide a process-based understanding of the relationship between solute transport and water saturation and can help to quantify the contributions of either factors on the overall solute mobility. Several pore-scale modeling studies have been conducted to calculate the effective diffusivity in porous media under saturated and unsaturated conditions (de Vries et al., 2017; Genty et al., 2017; Genty & Pot, 2014; Liu et al., 2020; Poonoosamy et al., 2022; Yang & Wang, 2019; M. Zhang et al., 2012). Given that pore-scale models require an explicit mesh based discretization of pore space, the solute

Core Ideas

- Solute transport in porous media at low water saturation is governed by the diffusion in thin water films.
- This study presents a modified pore-scale model involving the transport pathway in thin water films.
- A physically based formula is given to better predict the unsaturated effective diffusivity.
- A phase diagram is defined to identify the influence of surface water films on the effective diffusivity.

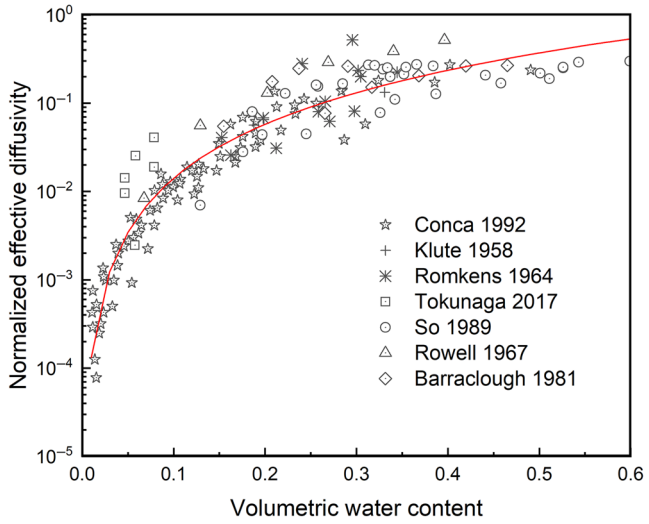

FIGURE 1 Experimental data of normalized effective diffusivity D_e^* measured in various soils as a function of the volumetric water content φ (Barraclough & Tinker, 1981; Conca & Wright, 1992; Klute & Letey, 1958; Romkens & Bruce, 1964; Rowell et al., 1967; So & Nye, 1989; Tokunaga et al., 2017). The red line is the fitting curve with the experimental data by using Equation (2): $D_e^* = 1.51\varphi^{2.03}$ ($R^2 = 0.64$).

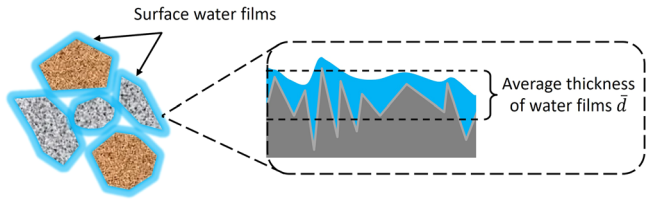

FIGURE 2 Surface water films with an average thickness $\bar{d}$ confined on the rough surfaces of solids.

transport in previous pore-scale simulations was mainly constrained by the classical percolation theory (Scher & Zallen, 1970; Zallen, 2008). However, at extremely low water saturation levels, classical percolation theory does not truly reflect the transport of solutes in unsaturated porous media. If we follow the classical percolation theory, the diffusive pathway is disconnected when the volumetric water content is below 0.05 ($\varphi < 0.05$) (D. P. Bentz & Garboczi, 1991). However, Tokunaga et al. (2017) reported that the diffusion pathways are still connected in unsaturated microporous media even at a volumetric water content as low as 10^{-4}. At such a low water saturation, the ultra-thin water films formed on the surface of soil particles, as illustrated in Figure 2, continue to provide a connective pathway for transport as reported by previous investigations (Conca & Wright, 1992; Hu & Wang, 2003). Moreover, the effective diffusivity in such media with low water saturation decreases rapidly due to the influences from both surface roughness and tortuosity of pores (Tokunaga et al., 2017).

The average thickness of water films $\bar{d}$ in unsaturated porous media relates to many factors such as saturation level, humidity, particle/pore size, and surface roughness, and ranges from several nanometers to a few micrometers (Carminati et al., 2008; Gao et al., 2021; Jiang et al., 2020; Lin et al., 2020; Tokunaga et al., 2017). When the thickness of the water film is in the order of some nanometers, the liquid–solid interface, especially the electrical double layer effect, will have a non-negligible impact on solute transport. However, this study focuses on microporous media (e.g., soils and sandstones) and a water content ensuring that the water films are confined in rough surfaces within a micro- and submicrometric thickness range (Jiang et al., 2020; Kasyap & Senetakis, 2018; Tokunaga & Wan, 1997). In such microporous media, the thickness of water films is usually smaller than the resolution of pore-scale simulations. Hence, it is difficult to resolve the water films in pore-scale models explicitly. Local mesh refinement may help to resolve the thin water films on the particle surfaces to a certain level but the computational costs will rapidly increase to a prohibitive level.

In order to improve the understanding of solute diffusion mechanisms in unsaturated microporous media, a method was developed to improve the pore-scale model explicitly accounting for the transport through surface water films without significantly increasing the computational costs. This model was applied to define the conditions under which the solute diffusion in water films is a significant or even the dominant solute transport mechanism. Finally, numerical results are upscaled and a theoretical assessment of the contribution from thin water films on the effective diffusivity of solutes in variably saturated microporous media is provided, which is validated with experimental data from Tokunaga et al. (Tokunaga et al., 2017).

2 | METHODS

In this study, the quartet structure generation set (QSGS) method based on the stochastic growth theory is used to generate three-dimensional microstructures of microporous media (Wang et al., 2007; Wang & Pan, 2008). By setting the growth factors, this method can control the statistical properties of reconstructed microstructures at the microscale (e.g., porosity, specific surface area, and mean particle size). Pore-scale modeling of solute diffusion in unsaturated porous media requires the following: (i) creating a precise static water–air phase distribution, and (ii) simulating the transport of the solutes in the aqueous phase. The lattice Boltzmann method (LBM) is a simulation method that allows for highly efficient parallelized computational algorithms and can address multiphase problems involving complex liquid–solid boundary conditions and interactions. Hence, it is often used to simulate the air–water distribution and the diffusion process at the

pore scale. For the first step, the two-phase single-component Shan-Chen LBM has been used in this study to simulate the spontaneous phase separation and to calculate the liquid/gas distribution in complex 3D pore geometries (Section 2.1). For the second step, a LBM for Fick's law has been used (Section 2.3). In addition, the model has been extended to account for thin water films during solute transport (Section 2.2).

2.1 | Lattice Boltzmann model for simulation of the static water–air distribution

The single-fluid two-component Shan-Chen lattice Boltzmann model was used to simulate the static water–air distribution in the pore structure (Shan & Chen, 1993, 1994). The formulation of the lattice Boltzmann evolution for this model is given by:

$$f_\alpha\left(r+\ c_f e_\alpha \delta t, t+\delta t\right)=f_\alpha\left(r,t\right)+\Omega_{bgk,\alpha}\left(r,t\right), \tag{3}$$

where f_α represents the particle distribution function along direction α, $\boldsymbol{r}$ denotes the position vector, δt the corresponding time step, and e_α the discrete velocities with discretized directions. $c_f=\delta x/\delta t$ is the lattice velocity for f_α and δx is the lattice size. In this study the three-dimensional nineteenth speed (D3Q19) lattice was used. In the Bhatnagar-Gross-Krook approach, the collision term $\Omega_{bgk,\alpha}$ is given as:

$$\Omega_{bgk,\alpha}=-\frac{\delta t}{\tau_f}\left(f_\alpha-f_{eq,\alpha}\right), \tag{4}$$

where τ_f is the dimensionless relation time and $f_{eq,\alpha}$ the equilibrium function. The equilibrium function is written as:

$$f_\alpha^{eq}\left(r,t\right)=w_\alpha\rho\left[1+\frac{3e_\alpha v}{c_f^2}+\frac{9\left(e_\alpha v\right)^2}{2c_f^4}-\frac{3v^2}{2c_f^2}\right], \tag{5}$$

where w_α is the distribution factor. For the D3Q19 lattice ($\alpha=0,1,2,\sim,18$), $w_\alpha=1/18$ for $\alpha=1-6$, $w_\alpha=1/36$ for $\alpha=7-18$, and $w_0=1/3$. ρ is the density of the fluid and v the velocity of the fluid defined by the equilibrium distribution function, which is different from the fluid velocity $u=v-\tau_f F_V/\rho$, where F_V is the external volumetric force. Fluid density and velocity can be obtained from the distribution function as $\rho=\sum_\alpha f_\alpha$, $u=(F_V\delta t)/(2\rho)+\sum f_\alpha e_\alpha/\rho$; the macroscopic kinematic viscosity v is related to the relaxation time: $v=c_f^2(\tau_f-\delta t/2)/3$. In the single component two phase Shan-Chen model, nonideal pressure during two component flow leading to phase changes is represented through a volumetric interaction force given by the following equation:

$$F_V\left(r,t\right)=-G\psi\left(r,t\right)\sum w_\alpha\psi\left(r+\ c_f e_\alpha\delta t,t\right)e_\alpha c_f/\sqrt{3}, \tag{6}$$

where G is the interaction strength taken as -120 in arbitrary nondimensional lattice units. ψ is the interaction potential given as:

$$\psi\left(\rho\right)=\psi_0\exp\left(-\rho_0/\rho\right). \tag{7}$$

In Equation (7), ψ_0 and ρ_0 are arbitrary constants. In this study, these constants are set to 4 and 200, respectively, such that for $G\ =-120$ phase separation would take place (Huang et al., 2015). Arbitrary parameters of Shan-Chen models can be related to various popular equations of state using the approach of Baakeem et al. (2020). However, for the purposes of the present study, this is not essential. For these set of parameters, the densities of the gas phase, ρ_g, and of the aqueous phase, ρ_w, are around 85.86 and 524.98 in arbitrary dimensionless lattice units with a density ratio between the two phases of around 6, which is significantly lower than the expected density ratio. Nevertheless, this difference in the density ratio is not critical for the flow in a rigid porous media (e.g., hardened cement paste) as demonstrated in J. Bentz et al. (2022). For the solid phase boundary condition, a previous study of Pot et al. (2015) indicated that the condition of a perfectly wetting surface agrees well with experimental observations. Hence, this study employed the same boundary condition that assumes water to be a perfectly wetting phase, and the solid phase was assigned the pseudo density of the water phase while computing the volumetric interaction force (J. Bentz et al., 2022). In addition, the classical bounce-back boundary condition in LBM is applied at the solid–fluid interface as a non-flux boundary condition normal to the solid surface. The periodic boundary condition is employed at all surfaces of the simulation domain. Details on the implementation of boundary conditions as well as on a consistent unit conversion between arbitrary dimensionless lattice units and physical units are described in Bentz et al. (J. Bentz et al., 2022). For this study, unit conversion is not relevant as only a simulation of the water distribution is carried out. To simulate the water distribution with the desired volumetric water saturation S_w, the initial condition is set using an equilibrium distribution function with a density $\rho=(1-S_w)\rho_g+S_w\rho_w$ and a fluid velocity equal to zero. The precise value of S_w are calculated after the simulation. The simulation is run until a steady state is reached, and the liquid and gas phase distributions are obtained using a threshold density equal to $0.5(\rho_g+\rho_w)$. Voxels with densities lower than the threshold density are considered as gas voxels and those with densities above as fluid voxels. Thus, at the end of the simulation, an output image consisting of three types of voxels—solid, water, and gas—is obtained. The described model was implemented in the open-source code Yantra (Patel, 2016, 2018).

In the microstructures of soils, it is difficult to resolve the water films by pore-scale models explicitly because the thickness of water films is usually smaller than the resolution of

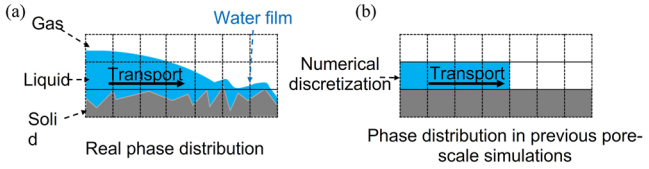

FIGURE 3 Phase distributions and transport pathways before numerical discretization (a) and after numerical discretization for pore-scale modeling (b). The existence of under-resolved water films is typically neglected.

pore-scale simulations. Figure 3a,b schematically illustrate this issue. For computing diffusivity, the output of single-component two-phase lattice Boltzmann models is processed such that a given single grid is treated as gas phase or liquid phase based on the density of the fluid (Pot et al., 2015; M. Zhang et al., 2012). This will eventually lead to depercolation of the water phase, and hence the porous medium will become non-diffusive and impermeable for solutes. This is illustrated in Figure 3a, where a continuous pathway from the left side to the right side exists for solute transport. However, since the thin water films cannot be resolved in a typical discretization used for the sake of computational efficiency and memory limitations, no transport of solutes can occur (Figure 3b). This disconnection caused by the numerical discretization is typical for under-resolved pore-scale simulations of unsaturated porous media reported so far in the literature. For instance, the simulations by Genty and Pot (2014) indicated that the diffusive pathway is disconnected in a porous medium consisting of packed spheres at $\varphi \approx 0.08$ and in a soil core at $\varphi \approx 0.05$. In the pore-scale simulation for cement paste, the effective diffusivity also reaches zero as φ decreases to 0.05 (M. Zhang et al., 2012).

2.2 | An improved approach to consider thin water films in solute transport

To overcome the limitation of the existing pore-scale simulations and to efficiently describe the subgrid water films, in this study, additionally, water-film grids are introduced at the gas–solid interface replacing the pure gas grids at these locations (red grids illustrated in Figure 4a) in the LBM model described in Section 2.1. On these grids, an equivalent diffusivity D_0^* (cf. Figure 4c) is used to calculate the corresponding flux across the grids by $\iint \boldsymbol{J}^{\text{num}}_{\text{water-film}} = \delta x^2 D_0^* \nabla C$ (mol/s). For simplicity, the average thickness $\bar{d}$ is employed for all water films on the surfaces of solid particles. Within the subresolution water film confined in the space of one grid (Figure 4b), the flux across grids is $\iint \boldsymbol{J}^{\text{real}}_{\text{water-film}} = \delta x \bar{d} D_0 \nabla C$(mol/s), assuming that these two cases are equivalent. Hence, as shown in Figure 4a,b, the fluxes $\boldsymbol{J}^{\text{num}}$ and $\boldsymbol{J}^{\text{real}}$ are equal under the same concentration gradient, leading to the following equation:

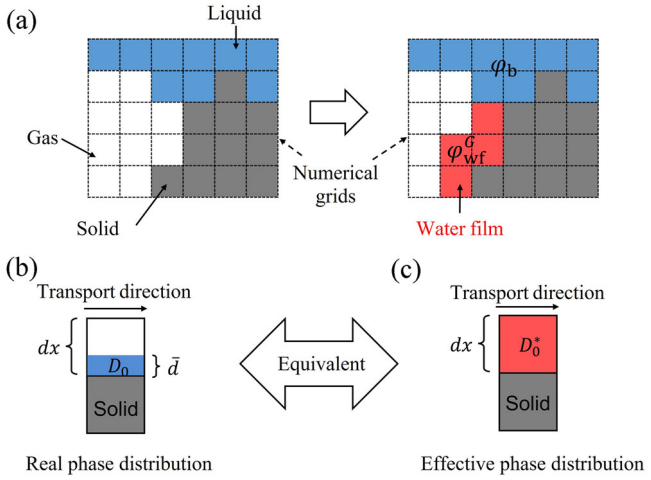

FIGURE 4 Schematic illustration of the two-dimensional discretized distributions of gas, liquid, and solid in the pore-scale simulations (a). The water-film grids (red) are added to replace previous gas grids (white) at the gas–solid interface. Fluxes are equivalent between the real phase distribution (b) and the effective distribution (c) with a reduced effective diffusivity D_0^*; the alteration of the water film thickness $\bar{d}$ is achieved by changing D_0^*.

$$\bar{d}\delta x D_0 \nabla C = \delta x^2 D_0^* \nabla C. \tag{8}$$

Therefore, the presence of a water film with a thickness $\bar{d}$ is reproduced by using an equivalent diffusion coefficient at the water-film grids:

$$D_0^* = \frac{\bar{d}}{\delta x} D_0. \tag{9}$$

Our study is primarily concerned with soils/porous media with a water content higher than 0.05. When the water content is below 0.05, the thickness of the water films could reach the nanometer scale (Tokunaga et al., 2017). In this situation, the nanoscale roughness of the surface and solid–liquid interfacial effects will have a critical impact on solute diffusion (Nishiyama & Yokoyama, 2021), where the non-linear relation of the diffusive flux to the thickness of the water film at each node will become significant.

In the proposed model, the water content φ consists of two parts: the bulk water content φ_b and the adsorbed surface water content φ_{wf}. Hence, the precise values of volumetric water content are recalculated after the simulations by: $\varphi = \varphi_b + \varphi_{wf} = \varphi_b + \varphi^G_{wf}\bar{d}/\delta x$, where φ^G_{wf} denotes the volumetric fraction of water film grids (red grids in Figure 4a). By following this approach, the pore-scale simulations can include the diffusive fluxes within the water films without the need to refine the mesh to resolve the local thin water films on the surface of the particles. Therefore, this methodology is computationally attainable without a computational overhead.

In order to avoid the average thickness of water films reaching nanoscale, this study focuses on microporous media with a

water content >0.05. In nature, it is common that the surfaces of coarser sand grains are coated with finer clay particles. Kasyap and Senetakis (2018) measured the roughness of sand grains coated with a clay agent. They found that the roughness of these surfaces ranged from 0.22 to 1.01 μm, based on different clay material concentrations. When the capillary forces dominate over the adsorptive forces for developing a water film, a previous theoretical study (Jiang et al., 2020) indicated that the average thickness of a water film on a microscale rough surface (e.g., sand grains coated with clay) is approximately equal to the surface roughness. When the water content of a sample reaches the minimum threshold of 0.05, it is assumed that the volume of water exclusively comprises the water films that uniformly coat the soil's rough surface. Tokunaga et al. (2017) also estimated an average thickness of water films ranging from 0.6 to 3.8 μm for sands with a water content close to 0.05. Hence, based on previous studies (Gao et al., 2021; Jiang et al., 2020; Tokunaga et al., 2017; Tokunaga & Wan, 1997) and the specific surface area of the digital soils, in this study we adopted two characteristic values of 1 and 4 μm as the average thicknesses of water films. Thus, the corresponding D_0^* was set equal to $0.05D_0$ and $0.2D_0$, respectively.

2.3 | Lattice Boltzmann model for simulation of solute diffusion

Since only nonvolatile solutes are considered in this study, the solutes can only diffuse in the aqueous phase governed by the classical Fick's law (Yoshida & Nagaoka, 2010):

$$\frac{\partial C}{\partial t} = \nabla \cdot J = \nabla \cdot \left(D_0 \nabla C \right), \tag{10}$$

where J, C, t, and D_0 denote the diffusive flux (mol/m^2/s), the aqueous solute concentration (mol/m^3), the time (s), and the diffusion coefficient in free water (m^2/s), respectively. When the simulations reach steady state, the effective diffusion coefficients are calculated by the flux through the unit cross section $\int J \mathrm{d}S/S$(Yang & Wang, 2018):

$$D_e = \frac{L}{C_{int} - C_{\text{out}}} \frac{\int J \mathrm{d}S}{S}, \tag{11}$$

where L is the domain length, C_{int} the solute concentration at the inlet, and C_{out} the concentration at the outlet (Figure 5).

Equation (10) is numerically solved by the LBM. Further computational details are summarized in Yang and Wang (2018). The corresponding numerical evolution function g_α is given as (Wang & Pan, 2008; Yoshida & Nagaoka, 2010):

$$g_\alpha \left(r + c_g \delta t_g e_\alpha, t + \delta t_g \right) - g_\alpha \left(r, t \right) = -\frac{1}{\tau_g} \left[g_\alpha \left(r, t \right) - g_\alpha^{eq} \left(r, t \right) \right], \tag{12}$$

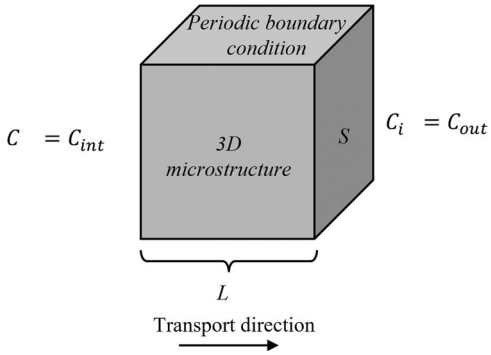

FIGURE 5 A sketch of the calculation domain and boundary conditions for solute diffusion.

where c_g is the lattice velocity for g_α and e_α represents the discrete velocities with discretized directions $\alpha = 0, 1, 2, \cdots 6$ for a three-dimensional seventh speed (D3Q7) scheme, since this scheme shows better stability and efficiency for diffusion simulations than the D3Q19 scheme (Yang & Wang, 2018). $\tau_g = 4D_0\delta t_g/\delta x^2 + 0.5$ is the dimensionless relaxation time. $g_\alpha^{eq} = \omega_\alpha C$ is the equilibrium distribution function with the distribution coefficients ($\omega_{\alpha=0} = 1/4$ and $\omega_{\alpha=1\sim6} = 1/8$) in the D3Q7 system. The local solute concentration at the pore scale is calculated by $C = \sum_\alpha g_\alpha$. Besides, the conventional bounce-back rule in LBM is employed as a zero normal flux boundary condition at liquid–solid or liquid–gas interfaces. Benefiting from the advantage of the LBM formulation, the local fluxes of solutes can be determined by $g_\alpha(r,t)$ at each grid as (Wang et al., 2007):

$$J_\beta = \frac{\tau_g - 0.5}{\tau_g} \frac{\delta x}{\delta t_g} \sum_\alpha \left(e_\alpha \cdot e_\beta \right) g_\alpha \left(r, t \right). \tag{13}$$

The diffusivity D_0 of the solute (e.g., NaCl) in free water was set to $2.0 \times 10^{-9}\ m^2/s$ at room temperature. The boundary concentrations at the inlet and outlet of the simulated domain are given as $C_{int} = 5.0 \times 10^{-2} mol/L$ and $C_{out} = 1.0 \times 10^{-2}\ mol/L$, respectively. The total diffusive fluxes through the porous media and the effective diffusivities are calculated using Equations (9)–(11) after a steady state has been achieved. Simulations without the consideration of water film were also conducted for comparison.

3 | RESULTS AND DISCUSSION

3.1 | Simulations of solute diffusion in digital microstructures of soils

The effective diffusivities of the partially saturated porous media were calculated in a series of 2 mm × 2 mm × 2 mm cubic microstructures of soils in which the porosity ranges

TABLE 1 Details of the reconstructed microstructures of digital soils (cross sections and pore size distributions are shown in Figure S1).

No.	Porosity	Specific surface area (mm^2/mm^3)	Size (mm^3)
S1	0.381	11.9	
S2	0.380	13.0	
S3	0.375	30.7	2×2×2
S4	0.599	8.7	
S5	0.599	21.3	

from 0.37 to 0.6. The details of these generated digital soils by the QSGS method are summarized in Table 1 and Figure S1, which are in the classical range of parameters for soils (Foth, 1991). Figure 6 shows an examplary cross section of microstructure (No. S1) and its pore size distribution. Since the maximum soil particle size is around 400 μm, this cubic microstructure can satisfy the representative elementary volume requirement based on our previous studies (Yang & Wang, 2018; Yuan et al., 2022). A 100 × 100 × 100 uniform numerical mesh with a lattice size of 20 μm was adopted for the LBM. It is noted that if one would try to discretize the same soil volume in a way to resolve the 1-μm water films, then a resolution of 1 μm instead of 20 μm would be needed. Such a simulation is practically impossible since it would need more than 8000 times larger computer memory and would be several orders of magnitude slower, especially when we consider that the simulation would need extremely more timesteps to converge.

3.2 | Importance of the diffusion in surface water films

The pore-scale model was used to simulate the steady diffusive processes in microporous media at different degrees of saturation. Figure 7a–d shows two examples of phase distribution and tracer concentration distribution in microstructure No. S4 at two different volumetric water contents of 0.17 and 0.4, respectively.

Figure 8 compares the simulations without water film with those considering water films with thicknesses of 1 and 4 μm, respectively (all simulation results are tabulated in Table S1). In general, our simulation results considering water films (blue and yellow lines) show better agreement with the best-fit curve (red line) from Figure 1 than those without the presence of the water films (black lines). When the volumetric water content exceeds 0.25, the water film and its thickness have little influence on the diffusive ion transport. Thus, the variances in the computed D_e^* between scenarios with water film thicknesses of 0, 1, and 4 μm were very small. However, at low volumetric water content (<0.15), the transport pathways in the absence of water films depercolate, which results in very low to no diffusive transport in the unsaturated media. In this situation, a conspicuous dissimilarity in the calculated D_e^* emerges between a water film thickness of 1 and 4 μm. This difference becomes larger as the water saturation decreases further. This demonstrates that the presence of water films on the solid surfaces controls the solute diffusion at low water contents. It is highlighted that contrary to standard practice, these processes need to be considered in pore-scale simulations to obtain a more realistic view on solute transport in partially saturated porous media. A sensitivity analysis of contact angle on the calculated D_e^* is also implemented in this study. The contact angle of water on soil surface should be below 90°. An extreme case with a contact angle of 90° is considered, and the results show that the change of contact angle up to 90° has only a limited impact on D_e^* for materials with a homogeneous water-wetting surface as shown in Figure S2.

3.3 | Theoretical analysis

The derived pore-scale numerical results were used to provide a comparative analysis that accounts for solute transport in variably saturated microporous materials. Based on the pore-scale numerical results, a theoretical (upscaled) model was derived to analyze the total flux J_{tot} of dissolved and non-volatile solutes as a function of φ_b and φ_{wf}, combining the bulk diffusion J_b and the surface-film diffusion J_s:

$$J_{tot} = J_b + J_s = -\varphi_b \tau_b^{-1} D_0 \nabla C - \varphi_{wf} \tau_s^{-1} D_0 \nabla C, \quad (14)$$

where τ_b and τ_s denote the tortuosity of diffusion in bulk water and along the solid surface, respectively. Assuming that tortuosity correlates to the corresponding volumetric fraction (Ghanbarian et al., 2013), Equation (14) can be modified by assuming a power law correlation into:

$$J_{tot} = -A\varphi_{wf}^{ns} D_0 \nabla C - B\varphi_b^{nb} D_0 \nabla C, \quad (15)$$

with four fitting parameters A, B, nb, and ns, which can be derived by fitting with the results of the pore scale simulations. φ_{wf} can be approximated by the surface area of the porous materials S and the average thickness of the water film $\bar{d}$ as $\varphi_{wf} = S\bar{d}$. φ_b is calculated through $\varphi_b = \varphi - \varphi_{wf}$; if $\varphi >> \varphi_{wf}$, $\varphi_b \approx \varphi$. Similarly, the effective diffusion coefficient of a solute can be derived from:

$$D_e = \left[A\left(S\bar{d}\right)^{ns} + B(\varphi)^{nb}\right] D_0. \quad (16)$$

The simulation cases that have zero bulk water content ($\varphi_b = 0$; cf. Table S1) only include the flux from surface-film diffusion J_s. Hence, Equation (15) can be reduced into

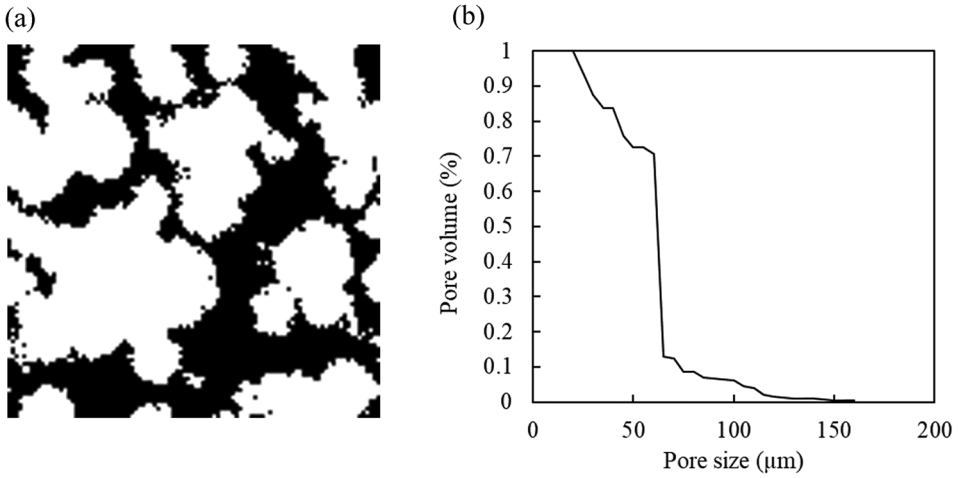

FIGURE 6 Cross section (a) of the digital microporous media S1 (white: solid phase; black: pore space; size: 2 mm × 2 mm) and corresponding pore size distributions (b).

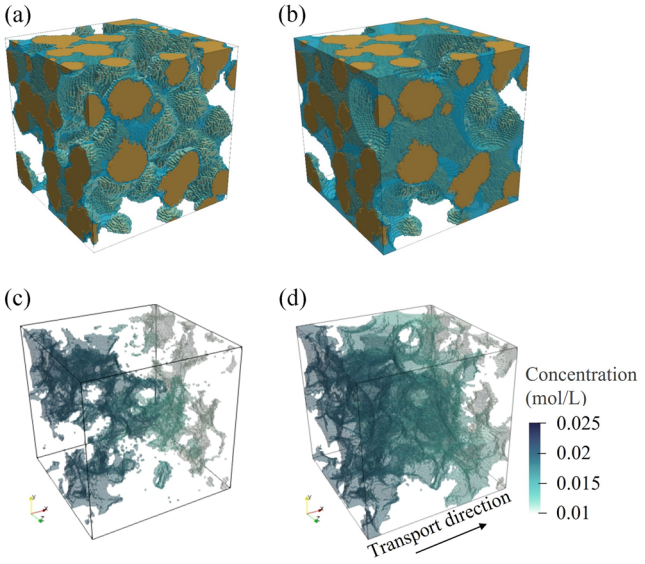

FIGURE 7 Gas–liquid–solid distribution in microstructure No. S4 (yellow: solid phase; blue: liquid phase; white: gas phase) at (a) low volumetric water content $\varphi = 0.17$, (b) high volumetric water content $\varphi = 0.40$, and (c and d) corresponding distributions of tracer concentrations within the liquid phase (only nonzero concentrations are visible).

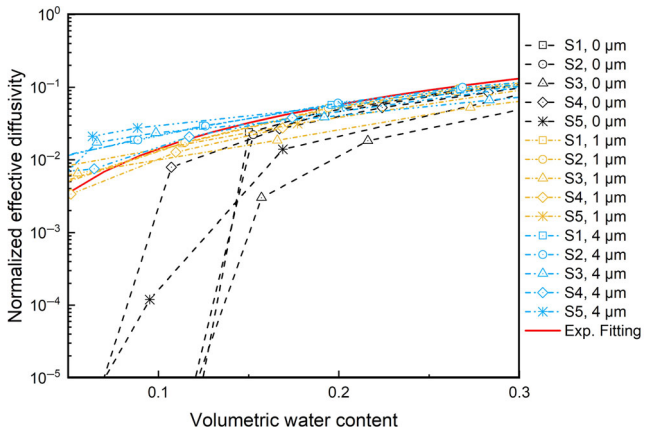

FIGURE 8 Comparison of simulated relative effective diffusivities of the generated soil microstructures for different water-film thicknesses as a function of the volumetric water content. Black lines: simulation results without water films (the classical pore-scale simulations); yellow lines: simulation results with 1-μm water films; blue lines: simulation results with 4-μm water films; the red line is the modified power law (Equation 2) fitted to the experimental datasets from Figure 1, that is, $D_e^* = 1.51\varphi^{2.03}$.

$J_{tot} = -A\varphi_{wf}^{ns} D_0 \nabla C = -A(S\bar{d})^{ns} D_0 \nabla C$. After fitting with the fluxes of the respective simulations, the fitting parameters are determined as $A = 0.17 \pm 0.13$ and $ns = 0.98 \pm 0.20$ ($R^2 = 86\%$) in Figure S3a. The values of $J_b = J_{tot} - J_s$ in the other cases can be calculated and fitted with the formula $-B(\varphi)^{nb} D_0 \nabla C$ to get $B = 1.17 \pm 0.27$ and $nb = 2.1 \pm 0.1$($R^2 = 97\%$). Figure S3b compares the normalized effective diffusivities for solute transport in bulk water derived from the pore scale simulations (as function of volumetric water content) to the fitting formula $-B(\varphi)^{nb}$. Since the new formula correlates D_e to S, $\bar{d}$, and φ, the fitting values (A, B, ns, and nb) are identical for the simulation results with different thicknesses of water film.

For comparison to the description of the effective diffusivity for transport in bulk water and in the water film (Equation 16), the parameters in the power law (Equation 2) were determined as $k = 0.40 \pm 0.10$ and $n = 1.20 \pm 0.11$ by fitting to the results of the pore scale simulations. The derived effective diffusivity by Equation (16) $J_{tot} = -[0.17(S\bar{d})^{0.98} + 1.17(\varphi)^{2.1}] D_0 \nabla C$ gave a better agreement to the diffusive flux than the power law $J_{tot} = -0.405\varphi^{1.2} D_0 \nabla C$ as shown in Figure 9. The average relative

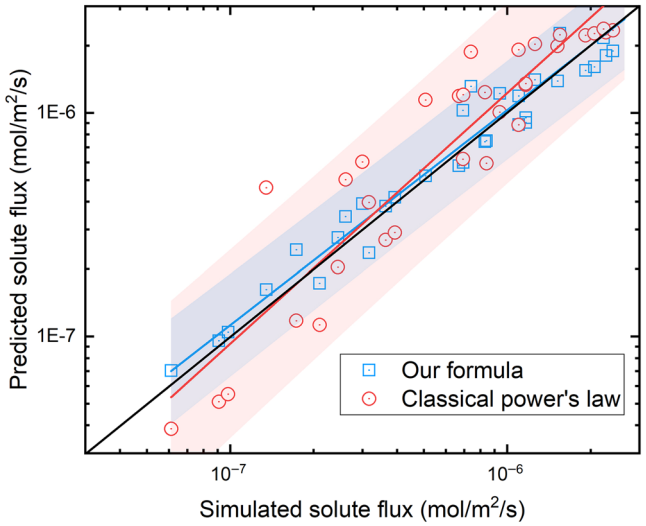

FIGURE 9 Comparison of solute fluxes (mol/m^2/s) in the digital soil microstructures simulated with the LBM pore scale model and derived from (i) our macroscopic equation (Equation 16; blue) and (ii) the power law (Equation 2; red) fitted with our pore-scale simulations (parameters $k = 0.405$ and $n = 1.2$). The shaded areas are 95% prediction bands from corresponding fitting lines.

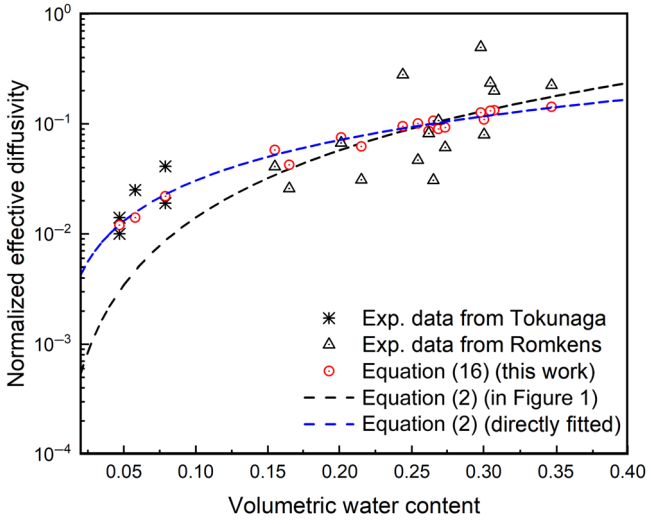

FIGURE 10 Comparison of experimentally measured normalized effective diffusivities (black stars) in quartz sands (Tokunaga et al., 2017) and glass beads/sand (Romkens & Bruce, 1964) to the predictions by classical power law from Figure 1 (Equation 2; black dashed line), directly fitted power law ($D_e^* = 0.51\varphi^{1.22}$; blue dashed line) and the macroscopic formula (Equation 16) developed in this work (red circles).

error of the classical power law with respect to the pore-scale simulations is 39.5%, while that of the derived macroscopic equation (Equation 16) is substantially reduced to 19.0%. Especially when the influence of the water film is critical ($\varphi < 0.15$), the average relative error of the classical power law increases to 52.5%. In contrast, the relative error of Equation (16) slightly decreases to 18.5% at these volumetric water contents.

To compare the performance of Equation (2) with that of the proposed Equation (16) in real soils, a blind prediction exercise was performed. Most data points at low water content in Figure 1 are given by Conca and Wright (1992). However, this study does not use their data points for this blind prediction because they measured the electric conductivity referring to D_e^*. Our newly introduced formula needs the specific surface area as the input. Hence, we estimated the volumetric-specific surface areas of the samples from Romkens and Bruce (1964) by using the mean particle size. We also directly fitted Equation (2) to selected experimental data, and derived $D_e^* = 0.51\varphi^{1.22}$, which is utilized for comparison. Table 2 compares previously measured values of D_e^* with our predictions. Solid/liquid interface effects such as the electrical double layer (EDL) effect may become nonignorable in porous media at extremely low water saturation, where the water film reaches the nanoscale, as already mentioned above. Since this interface effect will be involved in future studies, only data for quartz sands (Tokunaga et al., 2017) within the range $0.04 < \varphi < 0.1$ are used. In Figure 10, the normalized effective diffusivities, as predicted by the introduced formula $D_e^* = 0.17(S\bar{d})^{0.98} + 1.17(\varphi)^{2.1}$ (Equation 16), exhibit a better agreement with the measured values for quartz sands (Tokunaga et al., 2017) compared to the predictions by the modified power law $D_e^* = 1.51\varphi^{2.03}$ from Figure 1, while demonstrating comparable performance to the directly fitted formula $D_e^* = 0.51\varphi^{1.22}$. The predictions from all three formulae show a similar fitness with the experimental data from Romkens and Bruce (1964). Note that the use of Equation (16) does not depend on fitting to experimental data. The good agreement with experimental data validates our introduced formula in actual soils even though the parameters were obtained by the numerical structures. The proposed Equation (16) can be integrated into the classical continuum-scale reactive transport models to improve their predictions of reactive transport processes in partially saturated porous media. For example, by utilizing Equation (16), the continuum-scale model such as COMSOL Multiphysics can enhance the reliability of simulation of contamination diffusion in soils under low water saturation conditions.

Previous studies (Hu & Wang, 2003; Tokunaga et al., 2017) qualitatively stated that the relevance of the water film mainly depends on the volumetric water content, where the transport in water films dominates the total contributions to the solute flux below a critical volumetric water content. However, the importance of water films on transport has to be judged in conjunction with the porosity of the microporous media. For instance, for porous media having identical volumetric water content ($\varphi = 0.1$), in case of a material with a porosity $\theta = 0.2$, this volumetric water content would refer to a saturation of roughly $S_w = 0.5$, but in a coarser grained porous material

TABLE 2 Comparison of experimentally derived normalized effective diffusivities D_e^* for quartz sands (Tokunaga et al., 2017) and glass beads/sand (Romkens & Bruce, 1964) to those calculated by the modified power law $D_e^* = 1.51\varphi^{2.03}$ (Equation 2 in Figure 1), directly fitted power law $D_e^* = 0.51\varphi^{1.22}$ and by our macroscopic formula $D_e^* = 0.17(S\bar{d})^{0.98} + 1.17(\varphi)^{2.1}$ (Equation 16).

Solute	S(m^2/m^3)	$\bar{d}$ (μm)	φ	Experimentally measured D_e ($\times 10^{-11}$ m^2/s)	Experimentally measured D_e^*	D_e^* predicted by Equation (2) in Figure 1	D_e^* predicted by directly fitted Equation (2)	D_e^* predicted by Equation (16) (this work)
RbBr	1.13×10^5	0.55	0.058	5.07	0.025	0.005	0.016	0.014
RbBr	1.13×10^5	0.8	0.079	8.16	0.041	0.009	0.023	0.022
RbBr	1.13×10^5	0.8	0.079	3.78	0.019	0.009	0.023	0.022
RbBr	1.13×10^5	0.5	0.047	2.83	0.014	0.003	0.012	0.012
RbBr	1.13×10^5	0.5	0.047	1.91	0.010	0.003	0.012	0.012
NO_3^-	8.9×10^4	1.0	0.347	42.64	0.224	0.176	0.140	0.143
NO_3^-	8.9×10^4	1.0	0.300	15.15	0.080	0.131	0.117	0.109
NO_3^-	8.9×10^4	1.0	0.269	20.35	0.107	0.105	0.102	0.090
NO_3^-	8.9×10^4	1.0	0.273	11.60	0.061	0.108	0.105	0.093
NO_3^-	8.9×10^4	1.0	0.262	15.54	0.082	0.099	0.099	0.086
NO_3^-	8.9×10^4	1.0	0.215	5.88	0.031	0.067	0.078	0.062
NO_3^-	8.9×10^4	1.0	0.165	4.90	0.026	0.039	0.056	0.042
NO_3^-	1.98×10^5	1.0	0.155	7.76	0.041	0.034	0.052	0.058
NO_3^-	1.98×10^5	1.0	0.201	12.71	0.067	0.058	0.072	0.075
NO_3^-	1.98×10^5	1.0	0.244	53.15	0.280	0.086	0.091	0.095
NO_3^-	1.98×10^5	1.0	0.254	8.87	0.047	0.094	0.096	0.101
NO_3^-	1.98×10^5	1.0	0.265	5.84	0.031	0.102	0.101	0.107
NO_3^-	1.98×10^5	1.0	0.307	37.82	0.199	0.138	0.121	0.133
NO_3^-	1.98×10^5	1.0	0.305	44.68	0.235	0.135	0.119	0.131
NO_3^-	1.98×10^5	1.0	0.298	94.57	0.498	0.129	0.116	0.127

Note: The prediction of $\bar{d}$ is given from Tokunaga et al. (2017). The diffusivity of RbBr in free water is $D_0 = 2.0 \times 10^{-9}$ m^2/s and that of NO_3^- is $D_0 = 1.9 \times 10^{-9}$ m^2/s.

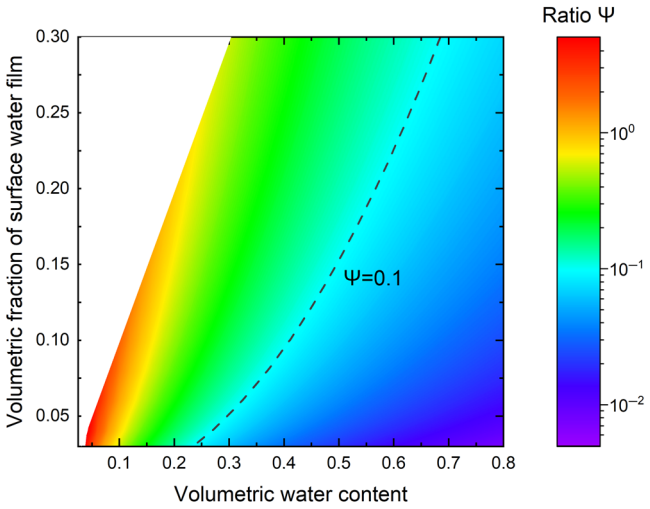

FIGURE 11 Phase diagram of the ratio $\Psi = J_s/J_b$ indicating the importance of diffusion in water films in terms of the volumetric water content and the adsorbed surface water content (cf. Equation 15). The black dashed line identifies the importance of diffusion in water films: the diffusion in water films is negligible on the right side of this line and becomes non-negligible on the left side. The white region is unachievable since the volumetric fraction of the surface water film would be larger than the total volumetric water content.

with porosity $\theta = 0.5$ and same volumetric water content, this would equal to a saturation level of $S_w = 0.2$. In consolidated clay rocks or even many sandstones and carbonate rocks, a volumetric water content of 0.1 would be close to full saturation. This means that the relevance of the water film does not only depend on the water content but also on the adsorbed surface water content in the surface water films. Therefore, we define a ratio, $\Psi = J_s/J_b$, between diffusional fluxes in the water film J_s and diffusional fluxes in the bulk water J_b; Ψ can be approximated by using Equation (15). A phase diagram of Ψ as a function of the volumetric water content φ and the adsorbed surface water content is plotted in Figure 11. This figure indicates the significance of diffusion within surface water films under different conditions in microporous materials, which can be important if $\Psi \approx 1$ or negligible if $\Psi < 0.1$. For example, the contribution of solute diffusion in water films can be ignored if $\varphi = 0.5$ and $\varphi_{wf} = 0.05$, while it becomes important at $\varphi = 0.1$ and $\varphi_{wf} = 0.05$.

4 | CONCLUSION

The diffusion of solutes through partially saturated geological materials such as soils and clay rocks is relevant in a wide variety of environmental processes. It is therefore important to predict how the water saturation affects the transport of solutes in porous materials. At this point, pore-scale simulations can quantitatively clarify the influences from different factors, such as surface area, porosity, and saturation level, on solute transport in partially saturated geological materials. Previous experimental investigations indicated that water films play a vital role in building a connecting pathway for solute transport at low water contents, where the classical percolation theory fails. However, previous pore-scale models could not resolve the thin water films on the rough surface of mineral particles due to numerical discretization issues. Hence, this study developed an improved method to improve the pore-scale framework to account for solute transport in thin water films and to consequently achieve a realistic description of solute transport in variably saturated microporous media, which is also helpful for the design and interpretation of future experiments.

The resulting simulation results allowed us to get an insight into the diffusive transport that takes place within the water films and its correlation with the overall effective diffusivity, as well as with the geometric characteristics of the simulated domains. By incorporating water films into a pore-scale model, the utilization of virtual synthetic structures allowed us to find a generic power law, particularly valid under conditions of water content higher than 0.05, which was successfully tested against two experimental datasets. Our introduced formula (Equation 16) can also be easily integrated into the classical continuum-scale reactive transport models to improve the reliability of simulations in unsaturated porous media. Future studies can quickly assess the contribution of thin water films on diffusive solute transport based on the straightforward phase diagram of $\Psi = J_s/J_b$ proposed in this study (cf. Figure 11).

This study focused on water films confined in rough surfaces of porous media within a micro- and submicrometric thickness range. However, other studies (Churakov, 2013; Savoye et al., 2012, 2014) indicated that the charged surfaces of clays also strongly affect solute diffusion in nanoscale water films. Besides, progressing desaturation in clay materials such as bentonite may additionally result in mechanical deformation of pore geometry (Xie et al., 2007; Xiong, 2020; C.-L. Zhang, 2021). These concepts are beyond the scope of application of this study. Further modeling and experimental studies are therefore needed to determine the influence of solid−water and water−gas interfaces as well as the chemical-mechanical coupling interaction on the transport of nanoconfined solutes in partially saturated porous media.

AUTHOR CONTRIBUTIONS

Yuankai Yang: Conceptualization; data curation; formal analysis; investigation; methodology; validation; writing—original draft; writing—review and editing. **Ravi A. Patel**: Investigation; writing—review and editing. **Nikolaos I. Prasianakis**: Supervision; writing—review and editing. **Sergey V. Churakov**: Supervision; writing—review and editing. **Guido Deissmann**: Funding acquisition; supervision;

writing—review and editing. **Dirk Bosbach**: Funding acquisition; project administration; supervision; writing—review and editing.

ACKNOWLEDGMENTS

We gratefully acknowledge funding by the German Federal Ministry of Education and Research (BMBF, grant 02NUK053A), the Innovation and Networking Fund of the Helmholtz Association (grant SO-093—iCross), and the European Union's Horizon 2020 Research and Innovation Programme (grant 847593 EURAD—DONUT). Yuankai Yang gratefully acknowledges the computing time granted through JARA on the supercomputer JURECA (Jülich Supercomputing Centre, 2021) at Forschungszentrum Jülich.

CONFLICT OF INTEREST STATEMENT

The authors declare no conflicts of interest.

ORCID

Yuankai Yang https://orcid.org/0000-0001-9550-2190
Guido Deissmann https://orcid.org/0000-0001-6039-9533

REFERENCES

Baakeem, S. S., Bawazeer, S. A., & Mohamad, A. A. (2020). Comparison and evaluation of Shan–Chen model and most commonly used equations of state in multiphase lattice Boltzmann method. *International Journal of Multiphase Flow*, *128*, 103290. https://doi.org/10.1016/j.ijmultiphaseflow.2020.103290

Badv, K., & Faridfard, M. R. (2005). Laboratory determination of water retention and diffusion coefficient in unsaturated sand. *Water, Air, and Soil Pollution*, *161*, 25–38. https://doi.org/10.1007/s11270-005-2444-6

Barraclough, P., & Tinker, P. (1981). The determination of ionic diffusion coefficients in field soils. I. Diffusion coefficients in sieved soils in relation to water content and bulk density. *Journal of Soil Science*, *32*, 225–236. https://doi.org/10.1111/j.1365-2389.1981.tb01702.x

Bentz, D. P., & Garboczi, E. J. (1991). Percolation of phases in a three-dimensional cement paste microstructural model. *Cement and Concrete Research*, *21*, 325–344. https://doi.org/10.1016/0008-8846(91)90014-9

Bentz, J., Patel, R. A., Benard, P., Lieu, A., Haupenthal, A., & Kroener, E. (2022). How heterogeneous pore scale distributions of wettability affect infiltration into porous media. *Water*, *14*, 1110. https://doi.org/10.3390/w14071110

Brooks, R. H., & Corey, A. T. (1966). Properties of porous media affecting fluid flow. *Journal of the Irrigation and Drainage Division*, *92*, 61–88. https://doi.org/10.1061/JRCEA4.0000425

Carminati, A., Kaestner, A., Lehmann, P., & Flühler, H. (2008). Unsaturated water flow across soil aggregate contacts. *Advances in Water Resources*, *31*, 1221–1232. https://doi.org/10.1016/j.advwatres.2008.01.008

Chou, H., Wu, L., Zeng, L., & Chang, A. (2012). Evaluation of solute diffusion tortuosity factor models for variously saturated soils. *Water Resources Research*, *48*, W10539. https://doi.org/10.1029/2011WR011653

Churakov, S. V. (2013). Mobility of Na and Cs on montmorillonite surface under partially saturated conditions. *Environmental Science & Technology*, *47*, 9816–9823. https://doi.org/10.1021/es401530n

Conca, J. L., & Wright, J. (1992). Diffusion and flow in gravel, soil, and whole rock. *Applied Hydrogeology*, *1*, 5–24. https://doi.org/10.1007/PL00010963

de Vries, E. T., Raoof, A., & van Genuchten, M. T. (2017). Multiscale modelling of dual-porosity porous media; a computational pore-scale study for flow and solute transport. *Advances in Water Resources*, *105*, 82–95. https://doi.org/10.1016/j.advwatres.2017.04.013

Fityus, S. G., Smith, D. W., & Booker, J. R. (1999). Contaminant transport through an unsaturated soil liner beneath a landfill. *Canadian Geotechnical Journal*, *36*, 330–354. https://doi.org/10.1139/t98-112

Foth, H. D. (1991). *Fundamentals of soil science* (8th ed.). Wiley.

Gao, H., Tatomir, A. B., Karadimitriou, N. K., Steeb, H., & Sauter, M. (2021). Effects of surface roughness on the kinetic interface-sensitive tracer transport during drainage processes. *Advances in Water Resources*, *157*, 104044. https://doi.org/10.1016/j.advwatres.2021.104044

Genty, A., Gueddani, S., & Dymitrowska, M. (2017). Computation of saturation dependence of effective diffusion coefficient in unsaturated argillite micro-fracture by lattice Boltzmann method. *Transport in Porous Media*, *117*, 149–168. https://doi.org/10.1007/s11242-017-0826-z

Genty, A., & Pot, V. (2014). Numerical calculation of effective diffusion in unsaturated porous media by the TRT lattice Boltzmann method. *Transport in Porous Media*, *105*, 391–410. https://doi.org/10.1007/s11242-014-0374-8

Ghanbarian, B., Hunt, A. G., Ewing, R. P., & Sahimi, M. (2013). Tortuosity in porous media: A critical review. *Soil Science Society of America Journal*, *77*, 1461–1477. https://doi.org/10.2136/sssaj2012.0435

Gimmi, T., & Churakov, S. V. (2019). Water retention and diffusion in unsaturated clays: Connecting atomistic and pore scale simulations. *Applied Clay Science*, *175*, 169–183. https://doi.org/10.1016/j.clay.2019.03.035

Hamamoto, S., Perera, M. S. A., Resurreccion, A., Kawamoto, K., Hasegawa, S., Komatsu, T., & Moldrup, P. (2009). The solute diffusion coefficient in variably compacted, unsaturated volcanic ash Soils. *Vadose Zone Journal*, *8*, 942–952. https://doi.org/10.2136/vzj2008.0184

Hasan, S., Niasar, V., Karadimitriou, N. K., Godinho, J. R. A., Vo, N. T., An, S., Rabbani, A., & Steeb, H. (2020). Direct characterization of solute transport in unsaturated porous media using fast X-ray synchrotron microtomography. *Proceedings of the National Academy of Sciences of the United States of America*, *117*, 23443–23449. https://doi.org/10.1073/pnas.2011716117

He, X., Guo, Y., Li, M., Pan, N., & Wang, M. (2017). Effective gas diffusion coefficient in fibrous materials by mesoscopic modeling. *International Journal of Heat and Mass Transfer*, *107*, 736–746. https://doi.org/10.1016/j.ijheatmasstransfer.2016.11.097

Hornung, U. (1997). *Homogenization and porous media*. Springer.

Hu, Q., Kneafsey, T. J., Roberts, J. J., Tomutsa, L., & Wang, J. S. Y. (2004). Characterizing unsaturated diffusion in porous tuff gravel. *Vadose Zone Journal*, *3*, 1425–1438. https://doi.org/10.2136/vzj2004.1425

Hu, Q., & Wang, J. S. Y. (2003). Aqueous-phase diffusion in unsaturated geologic media: A review. *Critical Reviews in Environmental Science and Technology*, *33*, 275–297. https://doi.org/10.1080/10643380390814488

Huang, H., Sukop, M., & Lu, X. (2015). *Multiphase lattice Boltzmann methods: Theory and application*. John Wiley & Sons.

Hunt, A. G., Ghanbarian, B., & Ewing, R. P. (2014). Saturation dependence of solute diffusion in porous media: Universal scaling compared with experiments. *Vadose Zone Journal*, *13*, 1–6. https://doi.org/10.2136/vzj2013.12.0204

Jiang, H., Guo, B., & Brusseau, M. L. (2020). Pore-scale modeling of fluid-fluid interfacial area in variably saturated porous media containing microscale surface roughness. *Water Resources Research*, *56*, e2019WR025876. https://doi.org/10.1029/2019wr025876

Jülich Supercomputing Centre. (2021). JURECA: Data centric and booster modules implementing the modular supercomputing architecture at Jülich Supercomputing Centre. *Journal of Large-Scale Research Facilities*, *7*, A182. https://doi.org/10.17815/jlsrf-7-182

Kasyap, S. S., & Senetakis, K. (2018). A micromechanical experimental study of kaolinite-coated sand grains. *Tribology International*, *126*, 206–217. https://doi.org/10.1016/j.triboint.2018.05.021

Klute, A., & Letey, J. (1958). The dependence of ionic diffusion on the moisture content of nonadsorbing porous media. *Soil Science Society of America Journal*, *22*, 213–215. https://doi.org/10.2136/sssaj1958.03615995002200030007x

Lin, X., Hu, Q., Chen, Z., Wang, Q., Zhang, T., & Sun, M. (2020). Changes in water vapor adsorption and water film thickness in clayey materials as a function of relative humidity. *Vadose Zone Journal*, *19*, e20063. https://doi.org/10.1002/vzj2.20063

Liu, C., Liu, Z., & Zhang, Y. (2020). A multi-scale framework for modelling effective gas diffusivity in dry cement paste: Combined effects of surface, Knudsen and molecular diffusion. *Cement and Concrete Research*, *131*, 106035. https://doi.org/10.1016/j.cemconres.2020.106035

Mehta, B. K., Shiozawa, S. H. O., & Nakano, M. (1995). Measurement of molecular diffusion of salt in unsaturated soils. *Soil Science*, *159*, 115–121. https://doi.org/10.1097/00010694-199502000-00006

Millington, R. J., & Quirk, J. P. (1961). Permeability of porous solids. *Transactions of the Faraday Society*, *57*, 1200–1207. https://doi.org/10.1039/TF9615701200

Nishiyama, N., & Yokoyama, T. (2021). Water film thickness in unsaturated porous media: Effect of pore size, pore solution chemistry, and mineral type. *Water Resources Research*, *57*, e2020WR029257. https://doi.org/10.1029/2020wr029257

Olesen, T., Moldrup, P., & Gamst, J. (1999). Solute diffusion and adsorption in six soils along a soil texture gradient. *Soil Science Society of America Journal*, *63*, 519–524. https://doi.org/10.2136/sssaj1999.03615995006300030014x

Patel, R. A. (2016). *Lattice Boltzmann method based framework for simulating physico-chemical processes in heterogeneous porous media and its application to cement paste*. Ghent University.

Patel, R. A. (2018). *Yantra: A lattice Boltzmann method based tool for multiscale/multiphysics simulations*. http://bitbucket.org/yantralbm/yantra

Poonoosamy, J., Lu, R., Lönartz, M. I., Deissmann, G., Bosbach, D., & Yang, Y. (2022). A lab on a chip experiment for upscaling diffusivity of evolving porous media. *Energies*, *15*, 2160. https://doi.org/10.3390/en15062160

Pot, V., Peth, S., Monga, O., Vogel, L. E., Genty, A., Garnier, P., Vieublé-Gonod, L., Ogurreck, M., Beckmann, F., & Baveye, P. C. (2015). Three-dimensional distribution of water and air in soil pores: Comparison of two-phase two-relaxation-times lattice-Boltzmann and morphological model outputs with synchrotron X-ray computed tomography data. *Advances in Water Resources*, *84*, 87–102. https://doi.org/10.1016/j.advwatres.2015.08.006

Qiu, C. Q., Han, J., Gao, H., Wang, L.-P., & Jin, Y. (2012). Pore-scale numerical and experimental investigation of colloid retention at the secondary energy minimum. *Vadose Zone Journal*, *11*, vzj2011–0071. https://doi.org/10.2136/vzj2011.0071

Raoof, A., Hassanizadeh, S. M., & Leijnse, A. (2010). Upscaling transport of adsorbing solutes in porous media: Pore-network modeling. *Vadose Zone Journal*, *9*, 624–636. https://doi.org/10.2136/vzj2010.0026

Revil, A., & Jougnot, D. (2008). Diffusion of ions in unsaturated porous materials. *Journal of Colloid & Interface Science*, *319*, 226–235. https://doi.org/10.1016/j.jcis.2007.10.041

Romkens, M., & Bruce, R. (1964). Nitrate diffusivity in relation to moisture content of non-adsorbing porous media. *Soil Science*, *98*, 332–337. https://doi.org/10.1097/00010694-196411000-00010

Rowell, D., Martin, M., & Nye, P. (1967). The measurement and mechanism of ion diffusion in soils III. The effect of moisture content and soil-solution concentration on the self-diffusion of ions in soils. *Journal of Soil Science*, *18*, 204–221. https://doi.org/10.1111/j.1365-2389.1967.tb01501.x

Savoye, S., Beaucaire, C., Fayette, A., Herbette, M., & Coelho, D. (2012). Mobility of cesium through the Callovo-Oxfordian claystones under partially saturated conditions. *Environmental Science & Technology*, *46*, 2633–2641. https://doi.org/10.1021/es2037433

Savoye, S., Imbert, C., Fayette, A., & Coelho, D. (2014). Experimental study on diffusion of tritiated water and anions under variable water-saturation and clay mineral content: Comparison with the Callovo-Oxfordian claystones. *Geological Society, London, Special Publications*, *400*, 579–588. https://doi.org/10.1144/sp400.9

Savoye, S., Page, J., Puente, C., Imbert, C., & Coelho, D. (2010). New experimental approach for studying diffusion through an intact and unsaturated medium: A case study with Callovo-Oxfordian argillite. *Environmental Science & Technology*, *44*, 3698–3704. https://doi.org/10.1021/es903738t

Scher, H., & Zallen, R. (1970). Critical density in percolation processes. *The Journal of Chemical Physics*, *53*, 3759–3761. https://doi.org/10.1063/1.1674565

Shan, X., & Chen, H. (1993). Lattice Boltzmann model for simulating flows with multiple phases and components. *Physical Review E*, *47*, 1815–1819. https://doi.org/10.1103/physreve.47.1815

Shan, X., & Chen, H. (1994). Simulation of nonideal gases and liquid-gas phase transitions by the lattice Boltzmann equation. *Physical Review E*, *49*, 2941–2948. https://doi.org/10.1103/physreve.49.2941

So, H., & Nye, P. (1989). The effect of bulk density, water content and soil type on the diffusion of chloride in soil. *Journal of Soil Science*, *40*, 743–749. https://doi.org/10.1111/j.1365-2389.1989.tb01314.x

Tokunaga, T. K., Finsterle, S., Kim, Y., Wan, J., Lanzirotti, A., & Newville, M. (2017). Ion diffusion within water films in unsaturated porous media. *Environmental Science & Technology*, *51*, 4338–4346. https://doi.org/10.1021/acs.est.6b05891

Tokunaga, T. K., & Wan, J. (1997). Water film flow along fracture surfaces of porous rock. *Water Resources Research*, *33*, 1287–1295. https://doi.org/10.1029/97wr00473

Wang, M., & Pan, N. (2008). Predictions of effective physical properties of complex multiphase materials. *Materials Science and Engineering: R: Reports*, *63*, 1–30. https://doi.org/10.1016/j.mser.2008.07.001

Wang, M., Wang, J., Pan, N., & Chen, S. (2007). Mesoscopic predictions of the effective thermal conductivity for microscale random

porous media. *Physical Review E*, *75*, 036702. https://doi.org/10.1103/PhysRevE.75.036702

Xie, M., Wang, W., De Jonge, J., & Kolditz, O. (2007). Numerical modelling of swelling pressure in unsaturated expansive elasto-plastic porous media. *Transport in Porous Media*, *66*, 311–339. https://doi.org/10.1007/s11242-006-0013-0

Xiong, Q. (2020). Discrete modelling of hydro-chemo-mechanical performance of clay materials. *Applied Clay Science*, *197*, 105760. https://doi.org/10.1016/j.clay.2020.105760

Yang, Y., & Wang, M. (2018). Pore-scale modeling of chloride ion diffusion in cement microstructures. *Cement and Concrete Composites*, *85*, 92–104. https://doi.org/10.1016/j.cemconcomp.2017.09.014

Yang, Y., & Wang, M. (2019). Cation diffusion in compacted clay: A pore-scale view. *Environmental Science & Technology*, *53*, 1976–1984. https://doi.org/10.1021/acs.est.8b05755

Yoon, H., Kang, Q., & Valocchi, A. J. (2015). Lattice Boltzmann-based approaches for pore-scale reactive transport. *Reviews in Mineralogy and Geochemistry*, *80*, 393–431. https://doi.org/10.2138/rmg.2015.80.12

Yoshida, H., & Nagaoka, M. (2010). Multiple-relaxation-time lattice Boltzmann model for the convection and anisotropic diffusion equation. *Journal of Computational Physics*, *229*, 7774–7795. https://doi.org/10.1016/j.jcp.2010.06.037

Yuan, T., Yang, Y., Ait-Mouheb, N., Deissmann, G., Fischer, C., Stumpf, T., & Bosbach, D. (2022). A comparative study on heterogeneity of clay rocks using pore-scale diffusion simulations and experiments. *Journal of Geophysical Research: Solid Earth*, *127*, e2022JB025428. https://doi.org/10.1029/2022jb025428

Zallen, R. (2008). *The physics of amorphous solids*. Wiley.

Zhang, C.-L. (2021). Deformation and water/gas flow properties of claystone/bentonite mixtures. *Journal of Rock Mechanics and Geotechnical Engineering*, *13*, 864–874. https://doi.org/10.1016/j.jrmge.2020.12.003

Zhang, M., Ye, G., & van Breugel, K. (2012). Modeling of ionic diffusivity in non-saturated cement-based materials using lattice Boltzmann method. *Cement and Concrete Research*, *42*, 1524–1533. https://doi.org/10.1016/j.cemconres.2012.08.005

SUPPORTING INFORMATION

Additional supporting information can be found online in the Supporting Information section at the end of this article.

How to cite this article: Yang, Y., Patel, R. A., Prasianakis, N. I., Churakov, S. V., Deissmann, G., & Bosbach, D. (2024). Elucidating the role of water films on solute diffusion in unsaturated porous media by improved pore-scale modeling. *Vadose Zone Journal*, *23*, e20321. https://doi.org/10.1002/vzj2.20321